Journal of Hazardous Materials 429 (2022) 128295

Contents lists available at ScienceDirect

Journal of Hazardous Materials

journal homepage: www.elsevier.com/locate/jhazmat

Research Paper

Latitudinal gradient for mercury accumulation and isotopic evidence for post-depositional processes among three tropical forests in Southwest China

Shangwen Xia [a,c,1], Wei Yuan [b,1], Luxiang Lin [a,c,f], Xiaodong Yang [a,c,*], Xinbin Feng [b], Xianming Li [d], Xu Liu [d], Peijia Chen [d], Shufang Zeng [d], Dingyong Wang [d], Qizhao Su [e], Xun Wang [b,**]

[a] CAS Key Laboratory of Tropical Forest Ecology, Xishuangbanna Tropical Botanical Garden, Chinese Academy of Sciences, Mengla 666300, Yunnan, China
[b] State Key Laboratory of Environmental Geochemistry, Institute of Geochemistry, Chinese Academy of Sciences, Guiyang 550081, China
[c] Center of Plant Ecology, Core Botanical Gardens, Chinese Academy of Sciences, Menglun, Yunnan 666303, China
[d] College of Resources and Environment, Southwest University, Chongqing 400715, China
[e] Mengla Institute of Conservation, Xishuangbanna Administration of Nature Reserves, Mengla 666300, Yunan, China
[f] National Forest Ecosystem Research Station at Xishuangbanna, Mengla 666300, Yunnan, China

HIGHLIGHTS

- The increasing surface soil mercury accumulation is observed along latitudinal gradient.
- Terrain and climate are main factors to drive the spatial distributions of tropical Hg.
- Microbial reduction mainly contributes to tropical Hg loss and isotopic fractionation.
- Atmospheric mercury net sink in tropical forests is likely much smaller than in other forests.

GRAPHICAL ABSTRACT

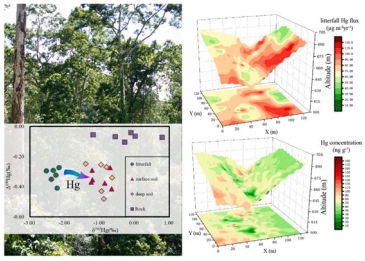

ARTICLE INFO

Editor: Dr. C. LingXin

Keywords:
Mercury isotope
Tropical forest
High resolution
Spatial distribution
Climate

ABSTRACT

Tropical forest contributes to > 50% of global litterfall mercury (Hg) inputs and surface soil Hg storage, while with limited understanding of Hg biogeochemical processes. In this study, we displayed the 5−m resolution of Hg spatial distribution in three 1-ha tropical forest plots across the latitudinal gradient in Southwest China, and determined Hg isotopic signatures to understand factors driving Hg spatial distribution and sequestration processes. Our results show that tropical forest at the lowest latitude has the highest litterfall Hg input (74.95 versus 34.14−56.59 μg m^{-2} yr^{-1} at higher latitude plots), but the smallest surface soil Hg concentration (2−3 times smaller than at higher latitude sites). Hg isotopic evidence indicates that the decreasing climate mediated microbial Hg reduction in forest floor leads to the increasing Hg accumulation along the latitudinal gradient in three tropical forests. The terrain induced indirect effects by influencing litterfall Hg inputs, soil organic matters distribution and interplays between surface and deep soils drive the heterogeneity of surface soil Hg distribution

* Corresponding author at: CAS Key Laboratory of Tropical Forest Ecology, Xishuangbanna Tropical Botanical Garden, Chinese Academy of Sciences, Mengla 666300, Yunnan, China.
** Corresponding author.
E-mail addresses: yangxd@xtbg.ac.cn (X. Yang), wangxun@mail.gyig.ac.cn (X. Wang).
[1] The authors contribute equally

https://doi.org/10.1016/j.jhazmat.2022.128295
Received 19 November 2021; Received in revised form 4 January 2022; Accepted 14 January 2022
Available online 19 January 2022

within each sampling plot. Our results highlight though the elevated litterfall Hg inputs, the distinct post-depositional reductions induced Hg loss would remarkedly decrease atmospheric Hg net sink in tropical forest.

1. Introduction

Ecological risks have aroused widespread concern, specifically the environmental pollution of organic pollutants and heavy metals (Lv et al., 2020; Yin et al., 2019). As a global pollutant, mercury (Hg) is emitted directly into the atmosphere from geogenic and anthropogenic sources and previously deposited Hg in natural surfaces (Driscoll et al., 2013; Obrist et al., 2018; Pirrone et al., 2010). There are three major forms of Hg speciation in the air, including gaseous element mercury (GEM), reactive gaseous mercury (RGM) and particulate bound mercury (PBM). RGM and PBM can deposit locally and quickly through precipitation and dry deposition into terrestrial ecosystems with a short atmospheric residence time of several days to weeks (Lindberg and Stratton, 1998; Lindqvist et al., 1991). Atmospheric GEM can transport long distance via the global atmospheric circulation with 0.5- to 1.5-year residence time (Lindberg et al., 2007; Lindberg and Stratton, 1998; Lindqvist et al., 1991; Obrist et al., 2018). Atmospheric Hg^0 uptake by vegetation then through litterfall deposition into the global terrestrial ecosystem is up to 1000–1200 Mg annually (Wang et al., 2016a). Recent studies suggested that using litterfall Hg deposition would underestimate the total atmospheric Hg^0 fluxes in the forests (Obrist et al., 2021; Wang et al., 2020b; Zhou and Obrist, 2021). Therefore, tracing Hg depositions and post-depositional sequestration in terrestrial ecosystems is critical for a complete understanding of global Hg cycling.

Mercury stable isotopes, which are quantified as mass dependent fractionation (MDF, reported as $\delta^{202}Hg$), even mass independent fractionation (even-MIF, reported as $\Delta^{200}Hg$ and $\Delta^{204}Hg$) and odd mass independent fractionation (odd-MIF, reported as $\Delta^{199}Hg$ and $\Delta^{201}Hg$), have been applied as useful tools to trace Hg sources and processes in forest ecosystems. In contrast to the Hg-MDF occurring during most of biogeochemical processes (Bergquist and Blum, 2007; Blum et al., 2014; Kritee et al., 2008, 2007; Sun et al., 2016), Hg odd-MIF can only take place in specific reactions, such as photoreduction (Bergquist and Blum, 2007; Sherman et al., 2010; Zheng and Hintelmann, 2009, 2010a), dark redox reaction and photo-oxidation (Sun et al., 2016). Distinct Hg even-MIF signatures, which are only observed in precipitation, are likely caused by photo-oxidation in the troposphere and relatively insensitive to other Hg biogeochemical processes (Chen et al., 2012; Demers et al., 2013; Gratz et al., 2010; Li et al., 2019). Therefore, tracing soil Hg sources by Hg stable isotopes has been accomplished in various forest ecosystems, and almost highlighted the vegetation uptake of atmospheric Hg^0 as the dominant source in forest floors (Guedron et al., 2018; Jiskra et al., 2015; Wang et al., 2017; Yuan et al., 2020; Zheng et al., 2016).

Tropical forests which account for 45% of the global forest areas (FAO, 2021) play an important role in global Hg cycles. Models estimate that tropical forests contribute to more than half of global litterfall Hg deposition and surface soil Hg storage (Wang et al., 2016a, 2019a). Several studies in Brazilian tropical forests have quantified the elevated atmospheric Hg depositions and soil Hg pool sizes (Carpi et al., 2014; Fostier et al., 2000, 2015; Melendez-Perez et al., 2014; Teixeira et al., 2012), however limited understanding in its biogeochemical processes and associated ecological risk remains. High temperature and humidity in tropical forest enhance an elevated biodiversity and nutrient turnover (Cavanaugh et al., 2014; Strassburg et al., 2010), thus likely leading to tropical Hg accumulation and sequestration different from Hg cycles in temperate and boreal forests. Wang et al. (2021) summarizes that the forest organic soil Hg pool size shows a logarithmic decrease with the increasing precipitation intensity across the globe, further suggesting a fast nutrient return that limits Hg accumulation in tropical forest soil. To current, few studies have conducted a comprehensive observation of Hg mass balance in tropical forests. Results identified by Hg isotopes in subtropical evergreen forests highlight that climate, vegetation and terrain factors shape Hg accumulation in forest floor (Lu et al., 2021; Yuan et al., 2021, 2020). However, the impacts of these issues on atmospheric Hg inputs through litterfall and Hg sequestration in tropical forests are still with large knowledge gaps.

In this study, we hypothesize that the climate mediated fast nutrient return and vegetation biodiversity in tropical forest would significantly influence Hg depositions and accumulation along the latitudinal gradient. In addition, Hg isotopic signatures in tropical forests would provide a useful tool to trace the Hg post-depositional processes, and to understand the variation of Hg accumulation in tropical forest floor. Therefore, we chose three typical tropical forests which located in the transection region of tropical to subtropical zone in Southwest China to demonstrate the variation of Hg accumulation in soils in response to the change of climate and vegetation. This is because meteorological factors and vegetation structures in the transection region are sensitive to the latitudinal shift. Given the elevated biodiversity in tropical forests, using several random sampling points to represent the Hg spatial distribution likely induces a distinct sampling bias. Herein, we used 1-ha sampling plot, which as the most widespread method for forest inventory, to assess Hg spatial accumulation in tropical forests. Finally, we discussed implications of tropical Hg biogeochemical processes in global Hg cycles.

2. Materials and methodology

2.1. Site description

We selected three tropical forests namely as Bu-Beng Forest Dynamics Plot (BB, 21° 36' 42.05" N, 101° 34' 57.72" E), P55 Forest Dynamics Plot (P55, 21° 57' 40" N,101° 12' 1.08" E), and Na-Ban-He Forest Dynamics Plot (NBH, 22° 7' 38.35" N, 100° 39' 39.96" E) in Xishuangbanna, Yunnan Province (Fig. 1). Although located in the transection region of tropical to subtropical zone, our selected forests are still as the tropical lowland rainforest since their typical tropical forest layers (i.e., emergents, the main canopy, under canopy and shrub layer) and typical tropical forest tree species (e.g., *Parashorea chinensis*, *Pometia pinnata*, *Cyclobalanopsis rex* and *Litsea pierrei*). The weather is as the tropical monsoon climate that up to 80% of total precipitation in rainy season (May−October). The mineral soil is oxisol soil with pH of 4−6, which comes from the weathered siliceous rocks (Cao et al., 2006). The BB has the elevation of 711–737 m, with a mean annual temperature of 22.5 ℃ and precipitation of 1650 mm (data from the Mengla meteorological station), and is dominated by tree species of *Parashorea chinensis* and *Litsea pierrei*. The P55 has the elevation of 725–766 m, with a mean annual temperature of 22.6 ℃ and precipitation of 1350 mm (data from Menglun meteorological station), and dominated by tree species of *Pometia pinnata* and *Barringtonia fusicarpa*. The NBH has the elevation of 751–806 m, with a mean annual temperature of 21.5 ℃ and precipitation of 1250 mm (data from Nabanhe Natural Reserver meteorological station), and dominated by species of *Pometia pinnata*, *Cyclobalanopsis rex* and *Litsea pierrei*. Given the warmer and wetter condition, the forest canopy height at BB is up to 60−65 m, while at P55 and NBH ranges between 30−45 m. Hence, the BB has the highest annual litterfall deposition flux with 1458 ± 367 g m^{-2} yr^{-1} (Mean±SD, n = 60), and then 1364 ± 272 g m^{-2} yr^{-1} at NBH, and finally 820 ± 78 g m^{-2} yr^{-1} at P55.

2.2. Sampling collection and pretreatment

We set a 1-ha sampling plot at BB, P55 and NBH (Fig. 1),

respectively. We collected litterfall samples in every 2-week starting from May 2018 to April 2019. The litterfall samples included litters of foliage, twigs and other detritus (e.g., flowers, seeds and mosses). The collection methodology has been documented in our earlier studies (Wang et al., 2016b, 2019b; Xia et al., 2015). Briefly, litterfall samples were collected by 1 m × 1 m nylon nets hanging 1 m above ground at 60 random locations in each sampling plot (Fig. 1). Litterfall samples were placed in paper bags and dried at 50 ℃ in an oven for 72 h. Our earlier studies have shown that this drying process would not lead to Hg loss from vegetation (Wang et al., 2016b). After being dried, litterfall samples were ground in an electric grinder and sieved with a 200–mesh (74 μm) sieve, and the fraction passed through the sieve was placed in Hg-free plastic bags for chemical analysis.

For surface soil samples, we set 100 subplots in our sampling plot (10 m × 10 m). In each subplot, four 1-m^2 sampling points within 5-m intervals were set (100 ×4 =400 surface soil samples, Fig. 1). Three replicate 0−10 cm depth soil cores were collected at each 1-m^2 sampling point, and mixed to produce a composite sample (1–2 kg in mass). In addition, 25 soil profiles were uniformly distributed (with ~25 m intervals between each, Fig. 1) in 1-ha sampling plot. We sampled the soil profile samples of 0–10, 10–20, 40–60, 60–80, 80–100 cm depth and deep rocks. All soil samples were stored in polythene bags, and then transferred to Soil Ecology Laboratory of the Xishuangbanna Tropical Botanical Garden. The soil samples were air dried and sieved following the same approach as the vegetation samples, and the < 74 μm fractions were placed in Hg-free plastic bags for chemical analysis.

2.3. Measurements

To display the impact of vegetation type on litterfall Hg concentration, we identified the tree species of collected litterfall samples in each sampling net. Then, we used the Direct Analysis Measurement 80 (DMA-80, detection limit: 1 ng g^{-1}) to analyze the vegetation and soil Hg concentrations. Standard reference materials of GBW07405 (GSS-5, soil, Hg = 290 ± 40 ng g^{-1}) and GBW10020 (GSB-11, vegetation, Hg = 150 ± 20 ng g^{-1}) were used for Quality Assurance/Quality Controller (QA/QC) and measured every 9 samples with a recovery of 95–105%. In addition, we utilized the Walkley-Back method (i.e., using $Cr_2O_7^{2-}$ to oxidize soil organic carbon, and then $FeSO_4$ to reduce the excess $Cr_2O_7^{2-}$) to determine soil organic carbon (SOC) content (Walkley, 1947).

We examined the Hg isotopic compositions of 3 high Hg concentration and 3 low Hg concentration surface soil samples in each forest plot to explore the relation between Hg concentrations and their isotopic compositions (Table S1–S4). We also measured the associated soil samples of 100-cm depth and rock samples to display the Hg isotopic signatures of geogenic Hg sources. Six litterfall sampling nets near the

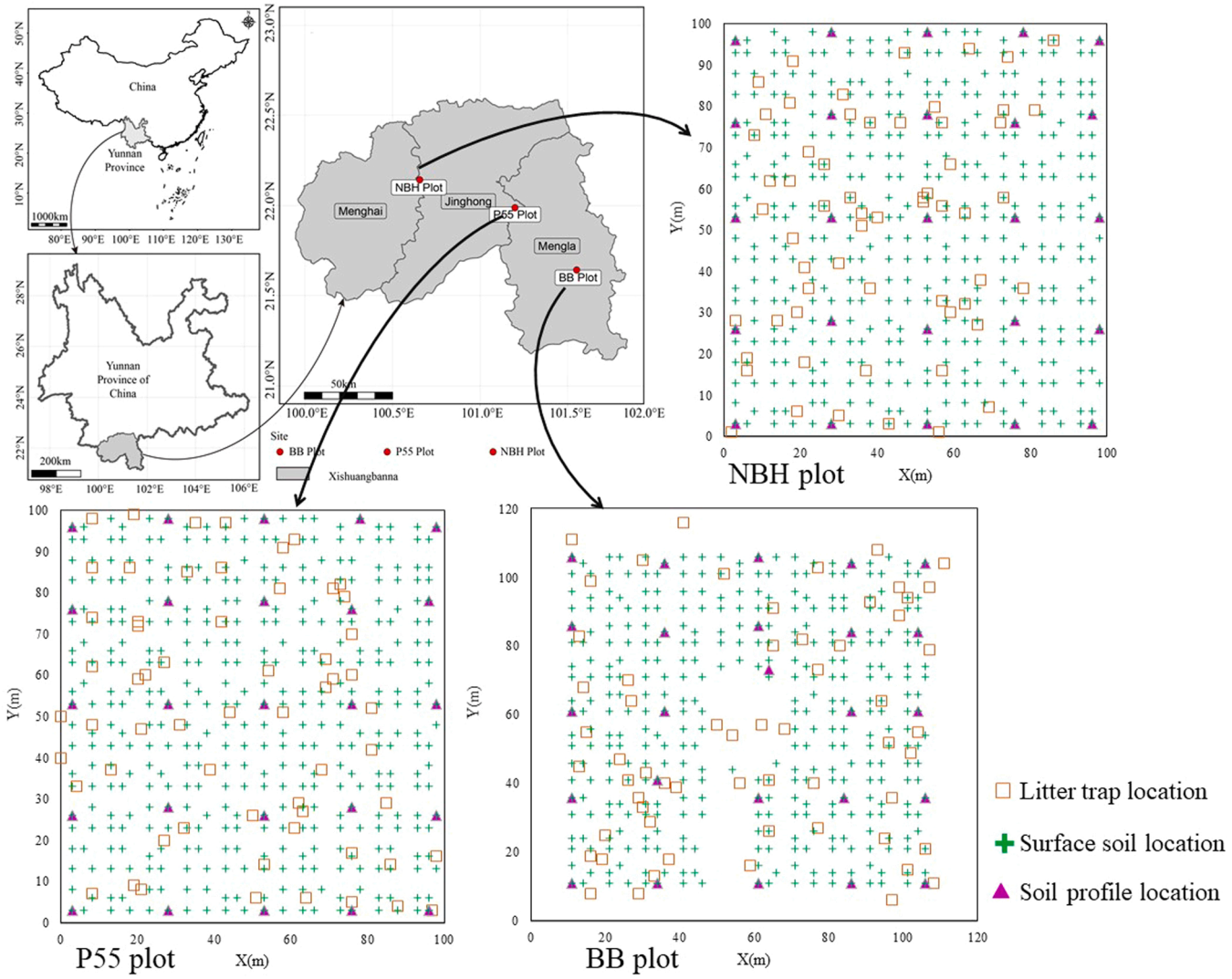

Fig. 1. Locations of three tropical forests and the methodology of sampling. We set a 1-ha sampling plot (central 100 m × 100 m in 1.44-ha plot) at BB, (100 m × 100 m) P55 and NBH.

selected soil sampling points in each forest were chosen and seasonal litterfall samples were mixed to produce 6 composite samples. We measured the Hg isotopic compositions of these composite samples to represent the average isotopic signatures of atmospheric litterfall Hg depositions.

The pre-concentration and Hg isotope measurements followed our previous works (Wang et al., 2017; Yuan et al., 2019), and were carried out at the State Key Laboratory of Environmental Geochemistry, Institute of Geochemistry, Chinese Academy of Sciences. Briefly, all samples were processed by double-stage heating pyrolysis in a tube muffle furnace with 5-mL oxidizing trapping solution of 40% mixture of concentrated nitric and hydrochloric acid ("reverse aqua regia", HNO_3: HCl = 2:1, v/v). The Hg concentration in trapping solution was analyzed by cold vapor atomic fluorescence spectrometry (Model 2500, Tekran® Instruments, Canada) following the protocol of US-EPA method 1631. The pre-concentration recovery was 98.2 ± 3.0% (n = 3) for a lichen standard reference material (BCR-482, 480 ± 20 ng g^{-1}) and 105.6 ± 3.5% (n = 3) for a certified soil reference material (GSS-4, 590 ± 50 ng g^{-1}). The Hg isotope compositions were measured by multi-collector inductively coupled plasma mass spectrometer (MC-ICPMS, Neptune II, Thermo Scientific, USA). The diluted trap solutions with 0.5 ng mL^{-1} and 3% $SnCl_2$ were introduced into a cold vapor phase separator, consistent with our laboratory earlier system (Fu et al., 2019). From Bergquist and Blum (2007), the MDF is reported as:

$$\delta^{202}Hg(‰) = \left[\left(^{202}Hg/\,^{198}Hg\right)_{sample} \Big/ \left(^{202}Hg/\,^{198}Hg\right)_{ref} - 1\right] \times 1000 \quad (1)$$

MIF is calculated as:

$$\Delta^{xxx}Hg(‰) = \delta^{xxx}Hg - \delta^{202}Hg \times \beta_{xxx} \quad (2)$$

where β_{xxx} is 0.252 for ^{199}Hg, 0.502 for ^{200}Hg and 0.752 for ^{201}Hg, respectively.($^{202}Hg/\,^{198}Hg)_{ref}$ represents the isotopic ratio in the standard sample (i.e., NIST-3133). BCR-482 and GSS-4 were combusted in the oven-enrichment system after every 10 samples were reproduced to assess whether the non-unity recoveries resulting from the double-stage offline combustion-trapping technique induced discernible isotopic bias. The Hg isotopic signatures for BCR-482 were measured as $\delta^{202}Hg$= −1.49 ± 0.03‰ , $\Delta^{199}Hg$= −0.62 ± 0.09‰ , $\Delta^{200}Hg$= 0.05 - ± 0.08‰ and $\Delta^{201}Hg$= −0.58 ± 0.12‰ (± 2σ , n = 3), and for GSS-4 as $\delta^{202}Hg$= −1.60 ± 0.05‰ , $\Delta^{199}Hg$= −0.46 ± 0.03‰ , $\Delta^{200}Hg$= 0. 00 ± 0.06‰ and $\Delta^{201}Hg$= −0.42 ± 0.06‰ (± 2σ , n = 6). The NIST-8610 was also analyzed for every 10 samples during the Hg isotope measurements, with isotopic signatures of $\delta^{202}Hg$= −0.50 ± 0.04‰ , $\Delta^{199}Hg$= −0.02 ± 0.04‰ , $\Delta^{200}Hg$= 0.02 ± 0.08‰ , Δ^{201}-Hg= −0.03 ± 0.05‰ (± 2σ , n = 7). The measured Hg isotopic signatures of these certified reference materials were consistent with recommended values, suggesting the validity of pre-concentration by using double-stage offline combustion-trapping.

2.4. Methods for statistical analysis

We used Nonparametric One-Way ANOVA, Independent Samples T-test and Paired Samples T-test to analyze statistical differences among the mean of Hg concentrations and their isotopic signatures in three tropical forests. The linear regression was used for statistical analysis among soil Hg concentration, soil organic matter, and Hg isotopes. To better understand the impacts of canopy structure on litterfall Hg concentration, we divided all tree species into three categories, as trees of canopy, understory and undergrowth. The canopy tree species is megaphanerophyte occupy which forms the emergent layer and canopy layer. The understory tree species is middle-size species occupy subcanopy layer, and undergrow layer tree includes dungarunga and shrubby species. In addition, we used the conceptual structural equation model to construct the interplays among terrain, litterfall Hg input, SOC, 100-cm depth soil Hg and surface soil Hg in three tropical forests. Structural equation model was developed by using χ^2 tests with maximum likelihood estimation, and more detailed information can be found in our earlier study (Wang et al., 2019a). Briefly, model fitting was performed by using SPSS version 17 and the Amos software version 24. The criteria for model optimization are based on the p-values (at least > 0.05), χ^2 values, and the Akaike information criterion (AIC). From the structural equation model path network, the standardized path coefficient (β) represents the direct effect of one variable on another, and the indirect effect is calculated by multiplying each associated β.

3. Results

3.1. Variations of litterfall Hg concentration and flux

The average Hg concentration in twig litter was 23.03 ± 11.58 ng g^{-1} at BB, 19.27 ± 3.97 ng g^{-1} at P55 and 10.48 ± 4.03 ng g^{-1} at NBH. The Hg concentration in debris (e.g., flowers, seeds and moss) was 61.29 ± 5.83 ng g^{-1} at BB, 53.73 ± 10.11 ng g^{-1} at P55 and 21.28 ± 3.51 ng g^{-1} at NBH. These Hg concentrations at NBH were significantly lower than those at the other two forest sites ($p < 0.05$, by Nonparametric One-Way ANOVA test, χ^2 =16.54 & 22.77, respectively). The total litterfall Hg concentration (including leaf litter, twig and debris) was 64.59 ± 2.56 ng g^{-1} for BB, 76.95 ± 3.04 ng g^{-1} for P55 and 72.94 ± 2.32 ng g^{-1} for NBH, with significant difference among each site ($p < 0.05$, by Nonparametric One-Way ANOVA test, χ^2 = 138.29). We observed the remarked inter-tree variabilities. The median litterfall Hg concentration was 68.72 ng g^{-1} with an IQR (i.e., interquartile range) of 51.48–84.90 ng g^{-1} at BB, and 87.79 ng g^{-1} with an IQR of 62.13–106.10 ng g^{-1} at P55, and 76.48 ng g^{-1} with an IQR of 63.69–90.37 ng g^{-1} at NBH (Fig. S1). In addition, the litterfall Hg concentration from canopy tree species was significantly lower than values from the understory layer and undergrowth layer tree species at BB and P55 ($p < 0.05$, by Nonparametric One-Way ANOVA test, χ^2 = 22.45 & 14.64, respectively; Fig. 2), but without significant difference at NBH. The litterfall Hg concentration at the three sites displayed insignificant seasonal variations (Fig. S2).

The litter Hg deposition flux was comparable between the dry and rainy seasons at BB (39.17 ± 10.34 μg m^{-2} versus 36.98 ± 10.99 μg m^{-2}; $p > 0.05$, Paired sample T-test) and P55 (15.40 ± 3.05 μg m^{-2} versus 18.74 ± 3.32 μg m^{-2}; $p > 0.05$, Paired sample T-test), but higher flux during dry season at NBH (36.84 ± 9.44 μg m^{-2} versus 19.76 ± 5.91 μg m^{-2}, $p < 0.05$ by Paired sample T-test). The litterfall Hg deposition flux from the canopy tree species was significantly higher than those from the other layers because of elevated biomass production ($p < 0.05$, by Nonparametric One-Way ANOVA test, χ^2 =53.63, 94.38, 24.15 for BB, P55, NBH, respectively; Fig. 2). Fig. 3a–c displayed the spatial distribution of litterfall Hg deposition. The litterfall Hg flux displayed a distinct spatial heterogeneity among three forests. The BB plot showed the highest spatial heterogeneity, and its litterfall Hg flux ranged between 4.48–118.81 μg m^{-2} yr^{-1}, followed by the NBH plot with a litterfall Hg flux of 33.83–90.80 μg m^{-2} yr^{-1}, and finally at P55 plot with 21.83–46.87 μg m^{-2} yr^{-1}. In addition, the high litterfall Hg flux point at the three sites almost scattered among the relatively slow slope and flat areas. The foliage Hg flux was the main fraction of total litterfall Hg depositions, accounting for 86% ± 7% of total depositions in dry season and 73% ± 9% in rainy season (Fig. 3d).

3.2. Variations of soil Hg distribution

Fig. 4a–c showed the spatial distribution of surface soil Hg in three tropical forests. The highest surface soil Hg concentration was at NBH, with a mean of 114.44 ± 27.68 ng g^{-1} (Median: 115.36 ng g^{-1} and IQR: 94.06–133.31 ng g^{-1}), followed by P55, with 79.53 ± 16.53 ng g^{-1} (Median:78.58 ng g^{-1} and IQR: 69.07 −87.74 ng g^{-1}), finally at BB, with 70.88 ± 15.98 ng g^{-1} (Median: 70.63 ng g^{-1} and IQR: 62.18–79.24 ng g^{-1}). The Hg concentrations between BB and P55 were comparable, but

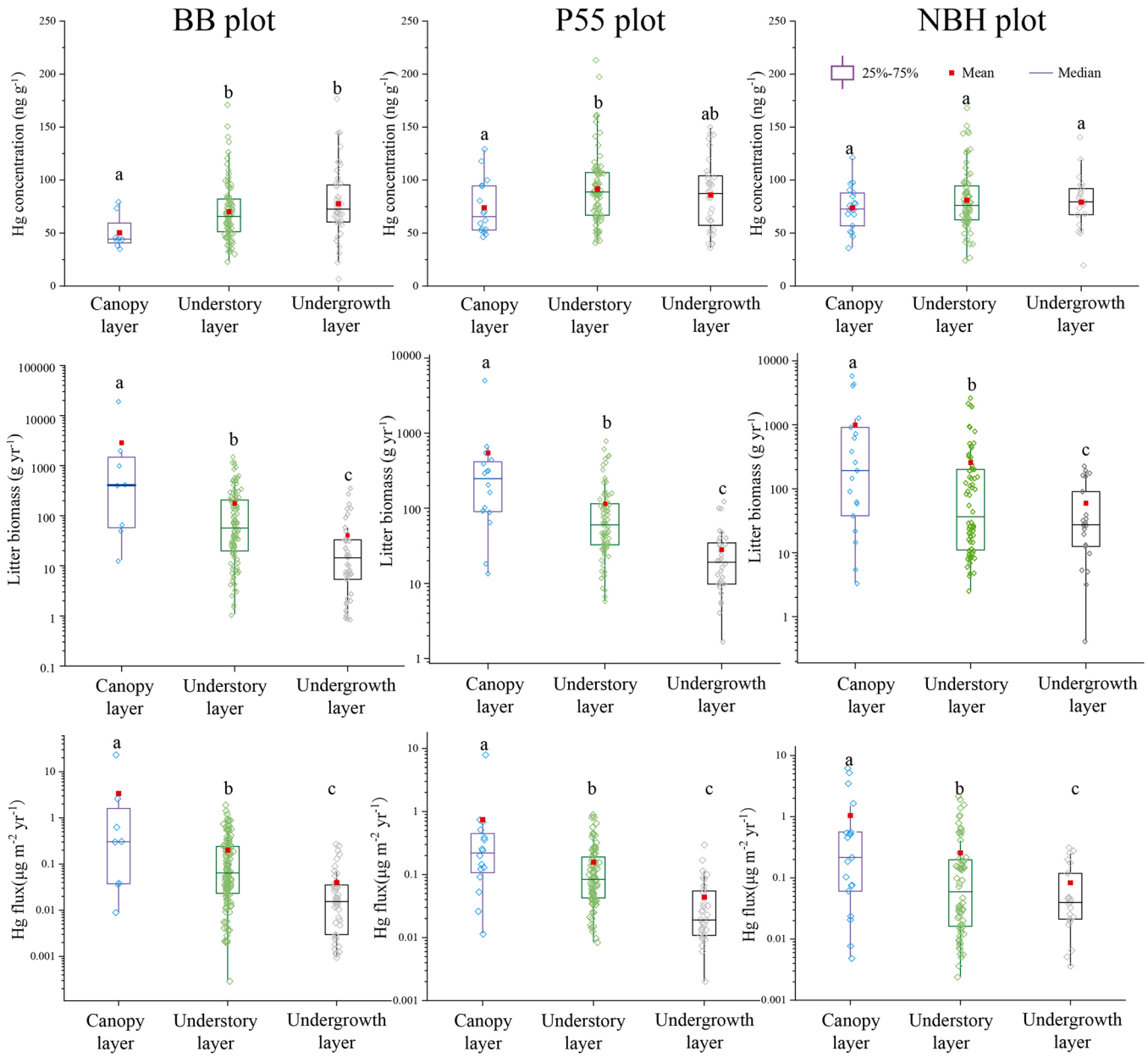

Fig. 2. Variations of Hg concentrations and fluxes among the canopy structures in three tropical forests. We used the letter (e.g., a, b, c) to represent the significant difference among three layers within each plot at the 95% confidence.

both were significantly lower than those at NBH ($p < 0.01$, Nonparametric One-Way ANOVA test, χ^2 =497.06; Fig. 4d). NBH and P55 had similar trend of spatial heterogeneity, that various high soil Hg points were mainly scattered among the slow slope and flat areas. The high soil Hg region at NBH distributed contiguously in the slow slope areas.

The Hg concentration showed a decreasing trend along with soil depth in the three tropical forests (Fig. S3). For the depth of 100-cm, the Hg concentration at BB was 1-fold lower than its surface soil Hg concentration (Figs. 5a-5d), with a mean of 32.89 ± 10.36 ng g^{-1} (Median: 34.79 ng g^{-1} and IQR: 26.04−39.31 ng g^{-1}). The Hg concentration of 100-cm depth soil was 58.55 ± 17.15 ng g^{-1} (Median: 55.69 ng g^{-1} and IQR: 47.97−68.63 ng g^{-1}) for P55, and 54.01 ± 27.42 ng g^{-1} (Median: 44.26 ng g^{-1} and IQR: 39.86−51.89 ng g^{-1}) for NBH. The soil Hg concentration at 100-cm depth showed a significantly positive correlation with the surface soil Hg concentration (R^2 =0.23, $p < 0.05$, Fig. S3d). Hence, the high Hg concentration regions in deep soils were consistent with surface soil Hg spatial distributions. In addition, all soil Hg concentrations showed a significant correlation with SOC (R^2 =0.38, $p < 0.05$, Fig. S4).

3.3. Variations of Hg isotopic signatures

The Hg isotopic compositions in litterfall showed comparable results in three tropical forests (Fig. 6a), as δ^{202}Hg= −2.31 ± 0.13‰ and Δ^{199}Hg= −0.32 ± 0.05‰ for BB (n = 6), δ^{202}Hg= −2.40 ± 0.15‰ and Δ^{199}Hg= −0.23 ± 0.05‰ for P55 (n = 6), and δ^{202}Hg= −2.17 ± 0.14‰ and Δ^{199}Hg= −0.35 ± 0.06‰ for NBH (n = 6). Although the surface soil Hg concentration was significantly higher than that in deep soil, the Hg isotopic signatures were comparable between surface and 100-cm depth soils. The Hg isotopic signatures were as δ^{202}Hg= −0.98 ± 0.27‰ and Δ^{199}Hg= −0.35 ± 0.05‰ for surface soil versus δ^{202}Hg= −0.94 ± 0.25‰ and Δ^{199}Hg= −0.34 ± 0.10‰ for deep soil at BB; δ^{202}Hg = −1.13 ± 0.14‰ and Δ^{199}Hg= −0.37 ± 0.06‰ for surface soil versus

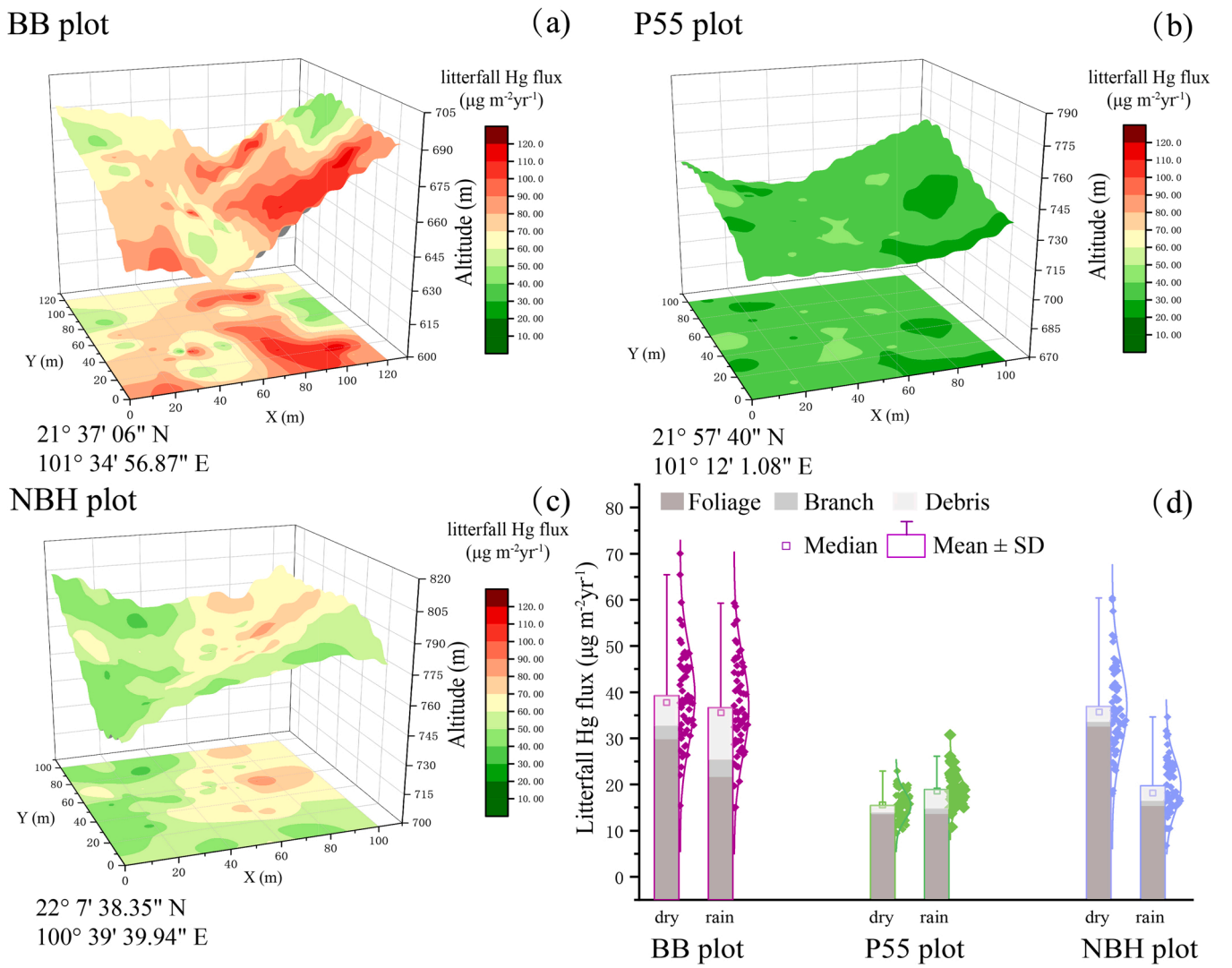

Fig. 3. Spatial distribution of litterfall Hg flux at BB (a), P55 (b) and NBH (c), and litterfall flux in dry and rainy seasons (d). The longitude and latitude of (0,0) in each sampling plot are marked in the figures.

δ^{202}Hg= −1.19 ± 0.14‰ and Δ^{199}Hg= −0.44 ± 0.07‰ for deep soil at P55; δ^{202}Hg= −1.24 ± 0.22‰ and Δ^{199}Hg= −0.43 ± 0.08‰ for surface soil versus δ^{202}Hg= −1.32 ± 0.11‰ and Δ^{199}Hg= −0.48 ± 0.10‰ for deep soil at NBH. The deep rock samples had the highest MDF and odd-MIF signatures, with δ^{202}Hg of − 0.22 ± 0.66‰ and Δ^{199}Hg of −0.07 ± 0.02‰ (n = 6). For Δ^{200}Hg, all samples showed close to 0.00‰ values (−0.04 ± 0.03‰). The Hg odd-MIF signatures in soils showed a negative correlation with soil Hg concentration (R^2 =0.21, $p < 0.05$, Fig. 6b).

4. Discussion

4.1. Factors influencing litterfall Hg input

Our litterfall Hg concentration is comparable to the value reported in other tropical forests (50 −90 ng g^{-1}), but significantly higher than that in temperate deciduous forests (30 −50 ng g^{-1}) (Blackwell and Driscoll, 2015; Demers et al., 2007; Fostier et al., 2015; Richardson and Friedland, 2015; Teixeira et al., 2017, 2012). This is attributed to the longer foliage lifespan and greater stomatal conductance of evergreen broadleaf facilitating a stronger Hg uptake rate (Wang et al., 2016b). The significantly negative odd-MIF signatures in our litterfall samples (Δ^{199}Hg: −0.23 ~ −0.35‰) are comparable to the global average odd-MIF signatures in litterfall (−0.30 ± 0.16‰, n = 123) and atmospheric Hg^0 (−0.16 ± 0.11‰, n = 343) (Wang et al., 2021). This suggests that the tropical litterfall Hg is mainly derived from atmospheric Hg^0 uptake, consistent with that in other forest ecosystems (Jiskra et al., 2015; Wang et al., 2017, 2020a, 2021, 2020b; Zheng et al., 2016).

Site BB has the highest canopy height (60−65 m) and biodiversity (166 tree species) due to the warm and wet climatic condition, when compared to P55 and NBH which with the canopy height of 30−45 m and 110−130 tree species. The litterfall Hg concentration of the same tree species among three sites shows insignificant differences ($p = 0.06$ −0.34, all $p > 0.05$ by Paired T-test). This suggests that a comparable atmospheric Hg^0 concentration at these remote tropical sites. However, the average of litterfall Hg concentration for all tree species at BB is significantly lower than other two sites, likely attributed to the tree-specific induced difference in atmospheric Hg^0 uptake.

Interestingly, litterfall Hg concentrations of canopy tree species are lower than values of other layer trees at BB and P55, but comparable Hg concentrations among different canopy layers at NBH (Fig. 2). We suggest that the climate induced the competitive regime could have consequences for different atmospheric Hg^0 uptake among canopy layers at BB and P55 (Ericksen et al., 2003; Frescholtz et al., 2003; Obrist et al., 2012; Rea et al., 2002; Teixeira et al., 2018). For tropical tree growing in a competitive regime (e.g., a warmer and wetter environmental

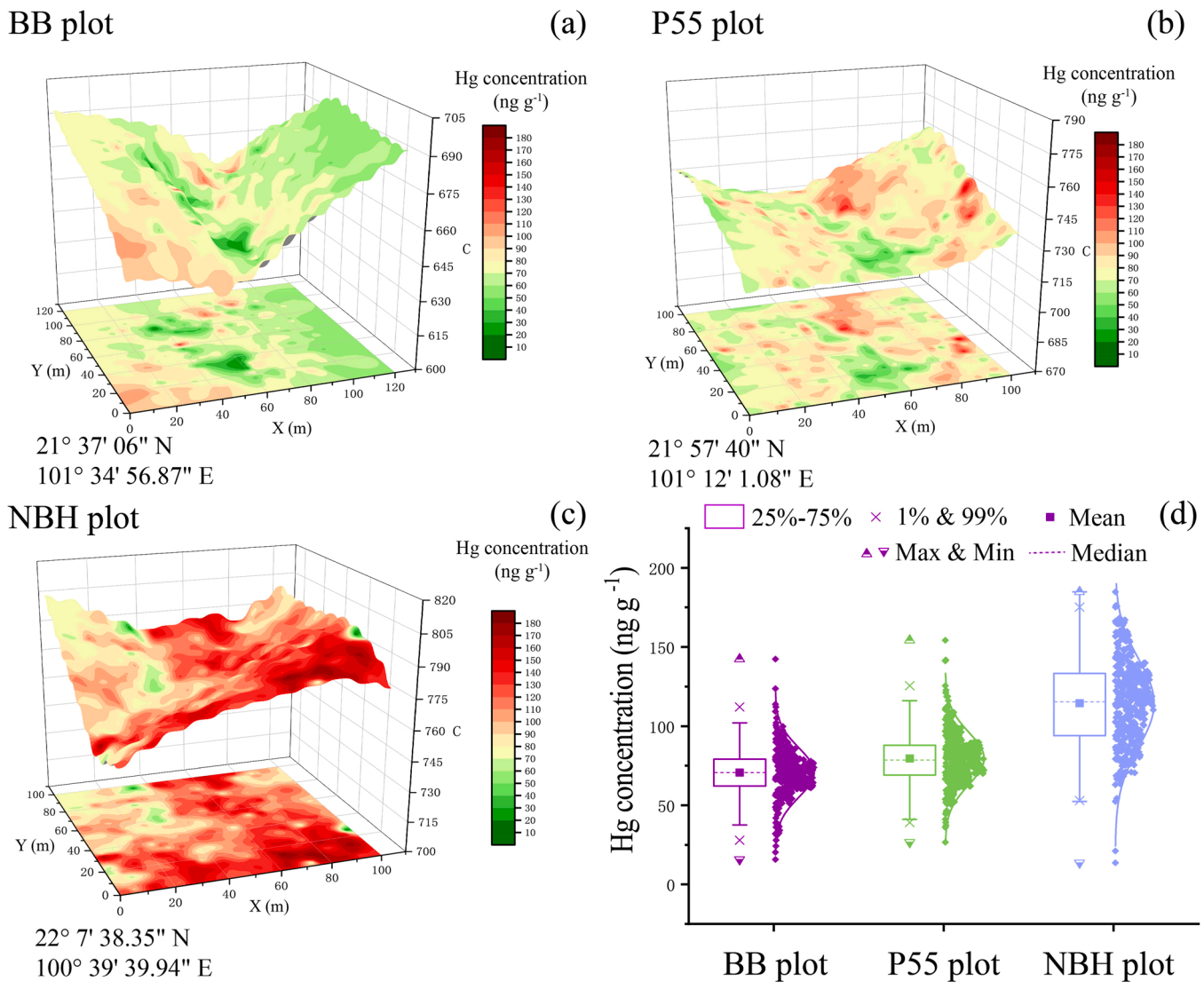

Fig. 4. Spatial distribution of surface soil Hg concentration at BB (a), P55 (b) and NBH (c), and box charts (d). The longitude and latitude of (0,0) in each sampling plot are marked in the figures.

condition at BB), strategies which maximize light efficiency or water efficiency will result in distinctly different structural and nutrient partitioning strategies (Kenzo et al., 2015; Lowry et al., 2021), thus influencing physiological parameters related to the atmospheric Hg^0 uptake. We recommend further studies to verify the correlation between physiological parameters and foliage Hg concentration among each layer tree species in tropical forests.

The mean litterfall Hg deposition flux (55.23 ± 21.96 μg m^{-2} yr^{-1}, IQR: 37.2 −69.97 μg m^{-2} yr^{-1}) is smaller than values in Amazon Basin tropical forests (84 ± 48 μg m^{-2} yr^{-1}, IQR: 47 −120 μg m^{-2} yr^{-1}) because of the smaller biomass production at our sites (Fostier et al., 2000, 2015; Silva et al., 2006; Teixeira et al., 2018). Though the litter Hg concentration of each tree species is diverse, the mixed litterfall Hg concentration in each sampling net does not exhibit consistent spatial distribution because of the mixing effect caused by high biodiversity of tropical forests. The elevated litterfall Hg deposition point is almost located at the slow slope or flat regions due to the terrain shaped the tree spatial distribution (Fig. 3). We observed the highest litterfall Hg deposition at BB, which is caused by much elevated litterfall biomass production (1458 ± 367 g m^{-2} yr^{-1} at BB, 820 ± 78 g m^{-2} yr^{-1} at P55 and 1364 ± 272 g m^{-2} yr^{-1} at NBH).

No seasonal trends of litterfall Hg deposition are at BB and P55, except NBH with a distinct seasonal trend that 45% higher deposition occurs in dry season. Given the leaf Hg deposition accounting for > 70% of total deposition, we suggest that the seasonal variation of leaf biomass is the key factor to determine such seasonal trend at NBH. Noteworthy, a trend of higher deposition in dry season is commonly observed in subtropical regions, due to the colder temperature and less precipitation provoking the leaf senescence (Liu et al., 2002; Lu et al., 2016). The NBH plot is located in the north areas of tropical to subtropical zone, thus exhibiting a similar seasonal trend of litterfall deposition observed in subtropical forests. The difference of seasonal variations among three sites mainly reflects the adoption strategies for tree species in response to the tropical to subtropical climatic transition.

4.2. *Factors influencing tropical Hg spatial distribution*

Our surface soil Hg concentrations are comparable to values in Amazon rainforests (106 ± 47 ng g^{-1}, Median: 93 ng g^{-1} and IQR: 83–131 ng g^{-1}) (Almeida et al., 2005, 2009; Melendez-Perez et al., 2014; Roulet et al., 1999, 1998). In this study, the elevated surface soil Hg points in each forest were not always associated with the high litterfall Hg input (Figs. 3 and 4). The spatial distribution of litterfall Hg input cannot solely explain the distribution of surface soil Hg (Figs. 3 and 4).

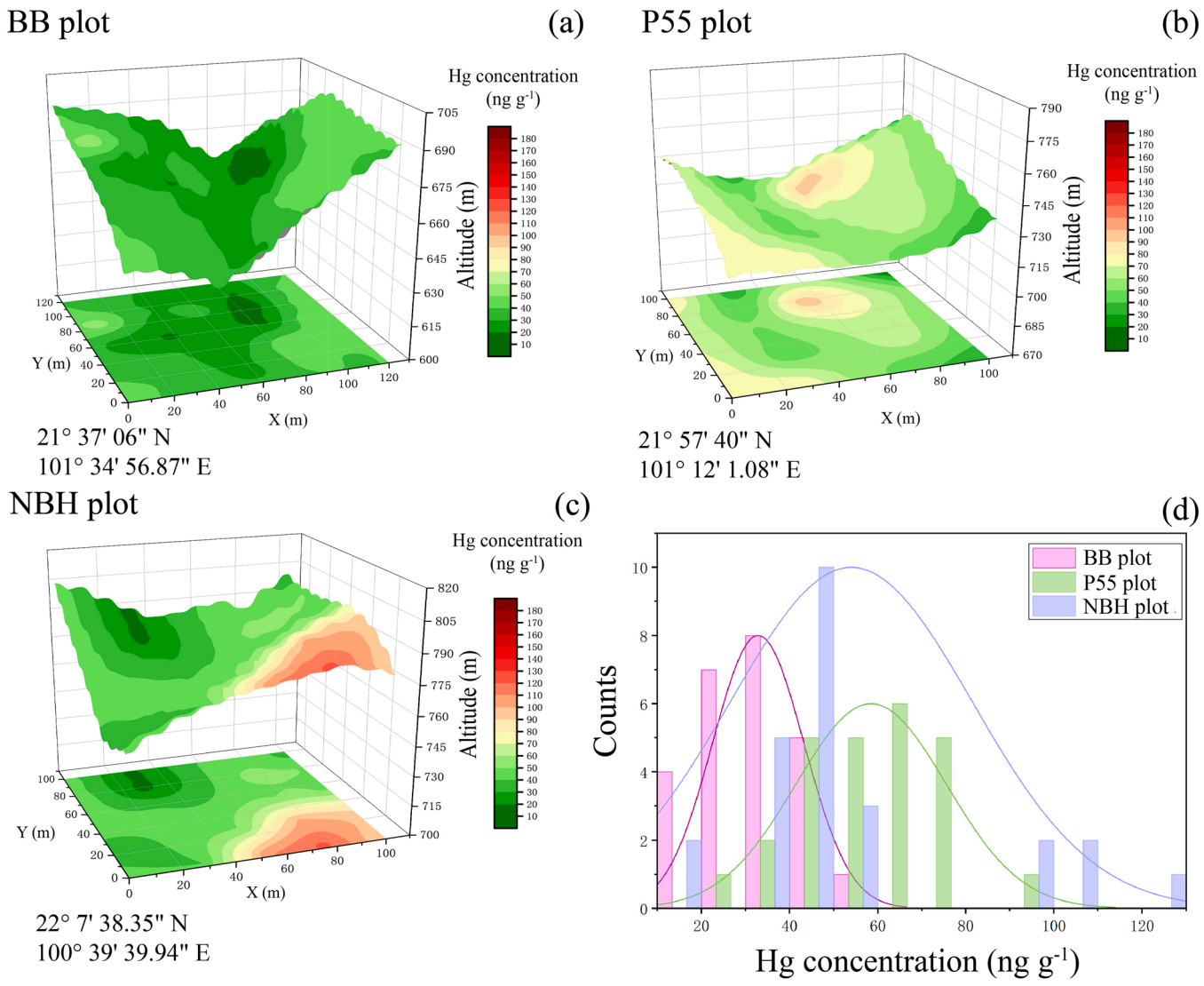

Fig. 5. Spatial distribution of 1-m depth soil total Hg concentration at BB (a), P55 (b) and NBH (c), and statistical frequency diagram (d). The longitude and latitude of (0,0) in each sampling plot are marked in the figures.

Specifically, the lowest latitude site (BB) has the highest litterfall Hg deposition, but the lowest surface soil Hg concentration; instead, the most north site (NBH) has the highest surface soil Hg concentration. To better explain the soil Hg spatial distribution, we used the structural equation model to quantify the contribution of litterfall Hg input, deep soil Hg (potential impacts from geogenic Hg sources or surface soil Hg leaching processes), and post-depositional processes.

Our structural equation model results can explain 55−60% of the variances in surface soil Hg concentrations at BB and NBH but 37% at P55, suggesting other unknown factors that need to be quantified by further research. Herein, we mainly discussed structural equation model results for BB and NBH. We used the elevation and TPI (topographic position index) to represent the impacts of terrain. This is because the value of elevation represents sample point absolute position, and TPI represents relative position against surrounded points. Table S5 and S6 further summarize that elevation, TPI, SOC, and deep soil Hg are the most important factors to shape surface soil Hg spatial distribution at BB and NBH.

The variation of terrain plays an important role in shaping the spatial distribution of litterfall biomass and Hg deposition (Fig. 7a−c). The standardized path coefficient (β) between TPI and litterfall biomass reaches the significant level at three sites, same for β between elevation and litterfall biomass at BB. These suggest the vertical elevation shift and variation of altitude against the neighbor point both influence the litterfall biomass production. Additionally, up to 0.5−0.9 of β values between litterfall biomass and Hg deposition flux at the three sites suggest the importance of biomass production to explain the variances in litterfall Hg deposition. Hence, the terrain has an indirect effect on litterfall Hg deposition by influencing biomass production.

For the surface soil Hg distribution, we found significant terrain impacts at BB, with β of −0.31 for elevation and 0.35 for TPI. This suggests the elevated surface soil Hg points were located in the low altitude and relatively slow slope regions at BB. It is noted that close to 0 for β between litterfall Hg input and surface soil Hg at BB, while ~0.2 at NBH. This indicates that despite the highest litterfall Hg inputs at BB, the elevated nutrient turnover induced the greatest Hg loss in forest floor (Lu et al., 2021; Wang et al., 2019b) likely leads to a smaller Hg accumulation at BB (more discussion in Section 4.3). The strong correlation between SOC and soil Hg concentration (Fig. S4d) reflects the complexation of Hg^{2+} with naturally occurring organics in soil (Obrist et al., 2009; Skyllberg et al., 2006). The β between SOC and surface soil Hg can represent the complicated effects of long-term litter decomposition. The highest β value (0.68) at BB suggests the residual Hg complexed with soil organic matters is more obvious at the wetter and

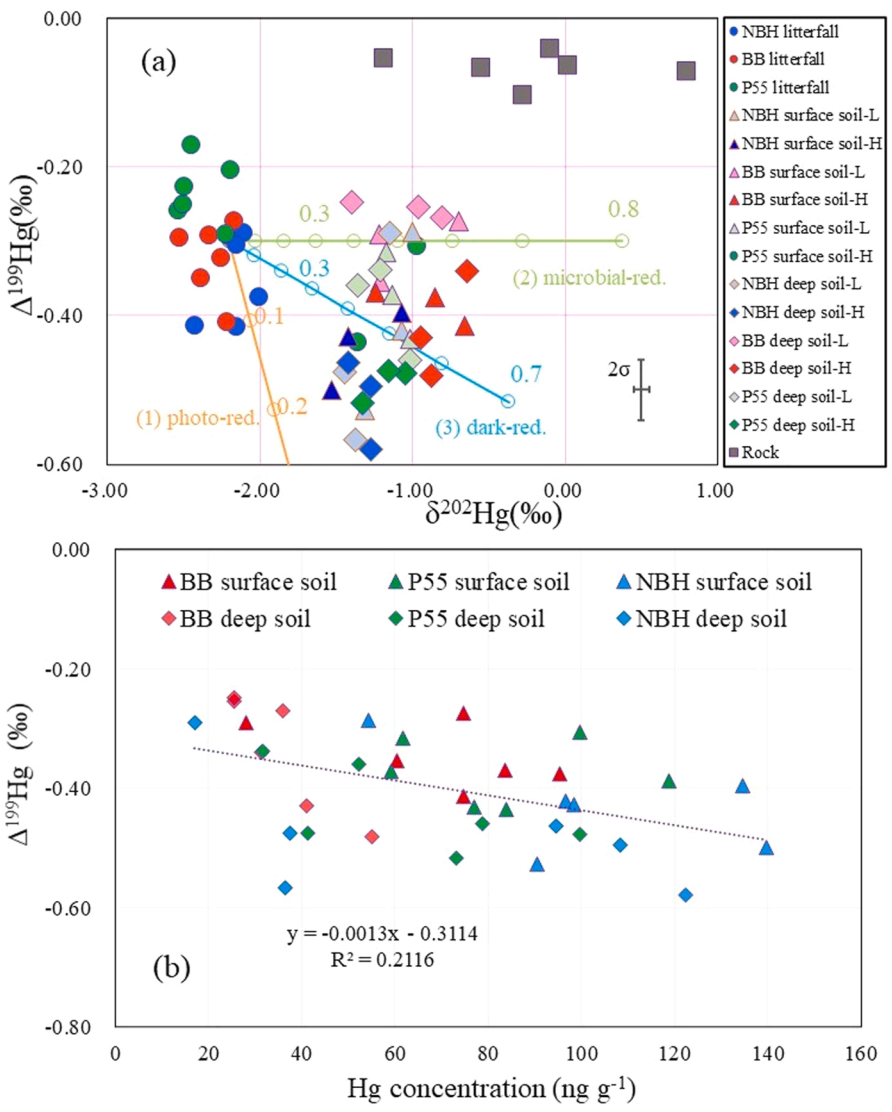

Fig. 6. (a) The Δ^{199}Hg versus δ^{202}Hg in three tropical forests; (b) soil Hg concentration versus Δ^{199}Hg signatures. "soil-H" represents the high soil Hg samples, and "soil-L" is the low soil Hg samples. The colorful lines represents trajectories for photochemical reduction (1 photo-red., in orange) (Zheng and Hintelmann, 2010a), microbial reduction (2 microbial-red., in light green) (Kritee et al., 2007) and abiotic dark reduction by natural organic matter (3 dark-red., in blue) (Zheng and Hintelmann, 2010b) with the respective fraction of reductive loss ($f_{reduced}$) based on the Rayleigh fractionation model (Jiskra et al., 2015). Error bar represents ± 2 standard deviation.

warmer site. The significantly positive β values along the path of elevation, SOC to surface soil Hg at NBH demonstrate the indirect impact of terrain on surface soil Hg distribution via influencing soil organic matter spatial distribution. Additionally, the significant β values along the path of TPI, deep soil to surface soil Hg at NBH suggest the distinct terrain mediated interplays between surface soil Hg and deep soil Hg (e.g., Hg leaching, geogenic Hg mixing), which further verified by using Hg isotopes. However, the negligible β values between deep soil and surface soil Hg at BB and P55 suggest few impacts from deep soil Hg.

Overall, we suggest the indirect effects of terrain on spatial distributions of litterfall Hg input and surface Hg concentration in each forest by influencing litterfall biomass, soil organic matters distribution, and interplays between surface and deep soil Hg. The latitudinal gradient of surface soil Hg distribution among three forests is likely controlled by the climate induced differences of Hg post-depositional processes, which discussed in detail by Hg isotopes in the following section.

4.3. *Isotopes showing Hg sequestration in tropical forest soils*

We used Hg isotopic signatures to display post-depositional Hg processes in soils. Three source endmembers have been identified for surface soil Hg, including atmospheric Hg^0 depositions, atmospheric Hg^{2+} depositions, and geogenic sources (i.e., weathering processes induce rock Hg release into soils). Given the significantly positive odd-MIF (Δ^{199}Hg=0.44 ± 0.23‰ and Δ^{201}Hg=0.42 ± 0.23‰) and even-MIF (Δ^{200}Hg=0.25 ± 0.19‰) in precipitation globally (Wang et al., 2021), the distinctly negative odd-MIF (−0.60‰ to −0.30‰) and the average of − 0.04‰ for even-MIF signatures in soils suggest that the atmospheric Hg^{2+} depositions have insignificant contribution. Compared to soil Hg, the rock exhibiting much positive Hg isotopic signatures (δ^{202}Hg=−0.22 ± 0.66‰, Δ^{199}Hg=−0.07 ± 0.02‰ and Δ^{200}Hg=−0.01 ± 0.04‰) suggests the rock weathering is not the main source for soil Hg accumulation. The soil Hg concentration in the 100-cm depth shows a significantly positive correlation to the surface Hg concentration (Fig. S3d), specifically at NBH. Such correlation can be attributed to the surface soil Hg leaching into the deep soil based on the Hg isotopic evidence. Fig. 6a clearly displays that the soil Hg odd-MIF signatures are close to values of litterfall, indicating the vegetation uptake of atmospheric Hg^0 dominating surface soil Hg sources. In addition, the throughfall Hg which also contains Hg derived from atmospheric Hg^0 sources (Wang et al., 2020b) can contribute to the tropical soil Hg accumulation. Finally, the previously deposited Hg re-emission is likely another important source for Hg accumulation in surface soil and litterfall.

The Hg reductive pathways induced enrichment factor of MDF ($\varepsilon^{202}Hg_{product/reactant} = \delta^{202}Hg_{product} - \delta^{202}Hg_{reactant}$) have been well documented. The $\varepsilon^{202}Hg_{product/reactant}$ during microbial reduction of Hg^{2+} is − 2.0‰ to − 1.2‰, and in organic matter dark-reduction is

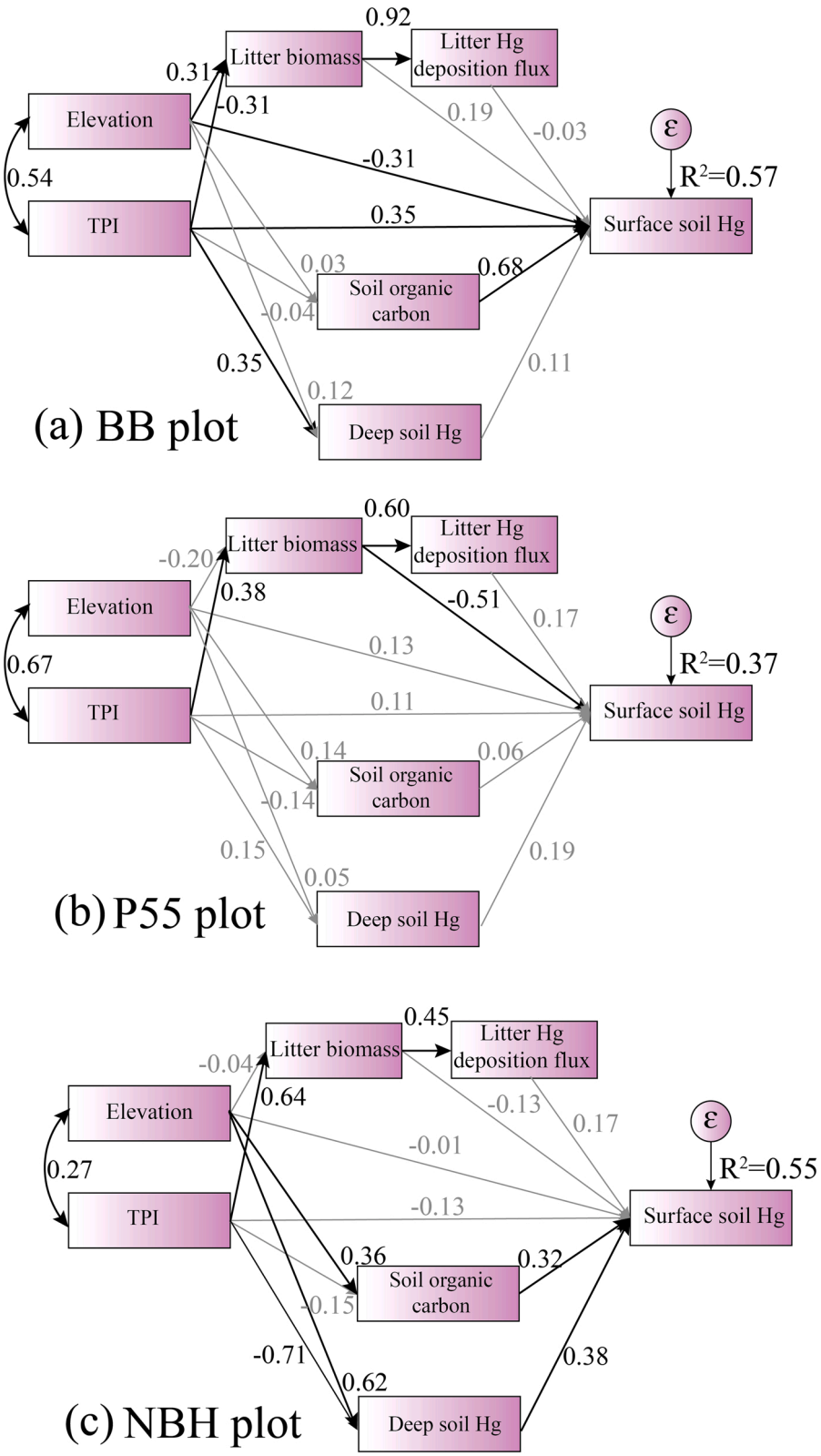

Fig. 7. Structural equation modeling fitted to surface soil Hg concentration among litterfall Hg deposition flux, litter biomass, elevation, TPI, soil organic carbon and deep soil Hg concentration at BB (a), P55 (b) and NBH (c). Numbers adjacent to arrows represent the standardized path coefficients. R^2 represents the proportion of variance explained. The grey arrows and numbers represent the insignificant effect at the 95% confidence level.

− 1.5‰ to − 1.7‰, and in photo-reduction is − 1.4‰ to − 0.6‰ (Bergquist and Blum, 2007; Kritee et al., 2008; Kritee et al., 2007; Rose et al., 2015; Zheng and Hintelmann, 2010a, 2010b). The microbial reductions have been regarded as the main cause for MDF in soils (Lu et al., 2021; Wang et al., 2019b). Fig. 6a exhibits the distinctly positive $\delta^{202}Hg$ shift between surface soil and litter ($\varepsilon^{202}Hg_{surfacesoil/litter} = \delta^{202}Hg_{surfacesoil} - \delta^{202}Hg_{litter}$), suggesting that the undergoing litter decomposing with the lighter isotope escaped preferentially. The highest $\varepsilon^{202}Hg_{surfacesoil/litter}$ is 1.33 ± 0.22‰ at BB, then 1.27 ± 0.22‰ at P55, and 0.94 ± 0.14‰ at NBH. Given the $\varepsilon^{202}Hg_{product/reactant}$ of microbial reductions, 55−65% of Hg loss at BB can lead to the similar value of $\varepsilon^{202}Hg_{surfacesoil/litter}$, ~55% at P55, and 40−50% at NBH based on the Rayleigh fractionation model (Jiskra et al., 2015). This can explain why the higher litterfall Hg depositions at BB but with lower soil Hg concentrations. The warmer and wetter environment at BB leads to the elevated decomposition rate which enhances the Hg loss via microbial reductions. The litterfall decomposition in subtropical forest has verified that higher decomposition rate would significantly increase the Hg loss (Li et al., 2022). The SOC and soil Hg contents in surface soil both decrease from NBH to BB, confirming the fastest litterfall decomposition and highest Hg loss at BB (Fig. S4). Additionally, the wetter and warmer condition at BB induced the higher Hg runoff and leaching are other possible causes for the Hg loss.

The microbial reduction of Hg^{2+} in soils would not induce the MIF (i.e., $E^{199}Hg_{product/reactant} = 0.00‰$) (Kritee et al., 2008, 2007). The close to 0.00‰ of $E^{199}Hg_{surfacesoil/litter}$ ($\Delta^{199}Hg_{surfacesoil} - \Delta^{199}Hg_{litter}$) at BB (−0.02 ± 0.06‰) further confirms the microbial reduction dominating the contribution of Hg loss. However, a small negative $E^{199}Hg_{surfacesoil/litter}$ value is found at P55 (−0.14 ± 0.08‰) and NBH (−0.08 ± 0.09‰), indicating the additional Hg reduction pathways occurred. The organic matter induced dark-reduction can produce of < −0.3‰ shift in residuals (Zheng and Hintelmann, 2010b). Given − 0.1‰ of $\Delta^{199}Hg$ shift in such dark-reduction with a 0.6 − 0.8‰ of $\delta^{202}Hg$ shift (Fig. 6a), We suggest the organic matter induced dark-reduction cannot solely explain the $E^{199}Hg_{surfacesoil/litter}$. This can be supported by several causes. One is that the occurring of organic matter induced dark-reduction could yield more positive $\varepsilon^{202}Hg_{surfacesoil/litter}$ at NBH and P55, however $\varepsilon^{202}Hg_{surfacesoil/litter}$ at two sites is significantly smaller than at BB. In addition, the slope of 1.1 between $\Delta^{199}Hg$ versus $\Delta^{201}Hg$ (Fig. S5) also suggest the small contribution from the organic matter induced dark-reduction which with a slope of 1.6 (Zheng and Hintelmann, 2010b). Moreover, the organic matter induced dark-reduction mainly occurs in the alpine and boreal forests (Jiskra et al., 2015; Yuan et al., 2020) due to the abundant organic matters caused by slow litter decomposition rate (several years to decades turnover). However, several months of litter decomposition induces a low organic matter level in tropical forest (Tuomi et al., 2009), thus likely limiting such dark-reduction.

Given atmospheric Hg^0 direct deposition occurring in forest floor, Hg^0 vapor dark oxidation by organic matter, which was observed with more negative MIF for products in the laboratory, has been suggested to cause $E^{199}Hg_{surfacesoil/litter} < 0$ (Zheng et al., 2019). However, the current filed measurements suggest the insignificant difference of Hg-MIF signatures during atmospheric Hg^0 deposition (Yuan et al., 2021). In addition, we did not observe distinct $E^{199}Hg_{surfacesoil/litter}$ at BB, although Hg^0 vapor dark oxidation by organic matter should occur commonly at three sites. Therefore, we suggest that Hg^0 vapor dark oxidation by organic matter would not significantly contribute to $E^{199}Hg_{surfacesoil/litter}$.

The slope of 1.1 between $\Delta^{199}Hg$ versus $\Delta^{201}Hg$ in soils suggests that MIF signatures are mainly derived from the photoreduction of Hg^{2+} (Fig. S5) (Bergquist and Blum, 2007). Upon UVB photolysis, Hg^{2+} complexed to thiol ligands in organic matter can yield a negative MIF in reactants (Motta et al., 2020; Zheng and Hintelmann, 2010a). Such photo-reduction processes can lead to 0.3−3.3 ng m^{-2} hr^{-1} Hg re-emission fluxes from subtropical forest floors (Yuan et al., 2021). The photoreduction of Hg^{2+} induced $\varepsilon^{202}Hg_{product/reactant}$ can be much smaller than the values from microbial reduction (Fig. 6a), consistent with a smaller $\varepsilon^{202}Hg_{surfacesoil/litter}$ at NBH and P55. Hence, we suggest the photo-reduction would contribute to such MIF shift in soils.

We observed the insignificant differences of Hg isotopic signatures between surface and deep soils in Fig. 6a, suggesting that Hg redoxes mainly occur in surface soils. This is different from another tropical study showing that the soil $\delta^{202}Hg$ signatures displayed a negative shift (−1‰) along with depth, which was attributed to a distinct MDF during Hg sorption and complexation onto iron oxides (Guedron et al., 2018). In addition, the soil Hg concentration showed a significant anti-correlation between the soil Hg concentration and $\Delta^{199}Hg$ signatures (Fig. 6b). This can be attributed that the slower turnover of nutrient leads to the higher residual Hg concentration at NBH and P55, and the following abiotic reductions (i.e., photo-reduction) to induce a small negative $\Delta^{199}Hg$ shift.

Our litterfall Hg deposition is 2−5 time higher than the documented depositions in temperate and boreal forests (10−20 μg m^{-2} yr^{-1}) (Wang et al., 2016a), however much shorter nutrient mineralization in tropical forests (Tuomi et al., 2009) leads to the elevated Hg loss during accumulation processes. This suggests that though much elevated litterfall Hg inputs, the net sink of atmospheric Hg in tropical forest would be much smaller than in other forests. Climatic factors significantly influence the tree physiological characteristics and nutrients turnover to control atmospheric Hg inputs and sequestration processes in forest floor. This indicates that the undergoing climate change would distinctly increase the unpredictability in assessing the effectiveness of Minamata Convention in controlling Hg pollution.

5. Conclusions

Along the latitudinal gradient of three tropical forests in Southwest China, this study comprehensively shows that the tropical forest at the lowest latitude has the highest litterfall Hg input but the smallest surface soil Hg concentration because of the elevated microbial reduction processes induced Hg loss. In addition, the slower turnover of nutrients in high latitude tropical forests would enhance the Hg abiotic reductions which inducing a small negative MIF shift in soils. The climate induced nutrient return and vegetation biodiversity dominantly drive the latitudinal gradient of Hg accumulation in forest floor. The terrain induced indirect effects on litterfall Hg inputs, soil organic matters distribution and interplays between surface and deep soils drive the heterogeneity of surface soil Hg distribution within each tropical forest. Our study suggests that fast nutrient cycles in tropical forests possibly lead to a smaller atmospheric Hg net sink than in other forests. We recommend further studies to quantify the tropical Hg mass balance and isotopic fractionation which offering a new insight in understanding tropical Hg cycling.

CRediT authorship contribution statement

Shangwen Xia and **Wei Yuan:** Investigation, Resources, Methodology Conceptualization, Formal analysis, Writing – original draft. **Xianming Li**, **Xu Liu**, **Peijia Chen**, **Shufang Zeng**, **Qizhao Su:** Investigation, Sampling, Data curation, **Xinbin Feng**, **Xiaodong Yang**, **Luxiang Lin** and **Dingyong Wang:** Writing – review & editing, Funding acquisition, **Xun Wang:** Conceptualization, Formal analysis, Methodology, Visualization, Data curation, Writing – original draft, Writing – review & editing, Funding acquisition.

Declaration of Competing Interest

The authors declare that they have no known competing financial interests or personal relationships that could have appeared to influence the work reported in this paper.

Acknowledgements

This work was funded by the National Natural Science Foundation of China (42122053, 42007307, and 42071074), and National Natural Science Foundation of China International (Regional) Cooperation and Exchange Program (42061144005). We appreciate the Xishuangbanna Station for Tropical Rain Forest Ecosystem Studies (XSTRE) for providing plot elevation, climate, tree species information and assistance in the field study.

Appendix A. Supporting information

Supplementary data associated with this article can be found in the online version at doi:10.1016/j.jhazmat.2022.128295.

References

Almeida, M.D., Lacerda, L.D., Bastos, W.R., Herrmann, J.C., 2005. Mercury loss from soils following conversion from forest to pasture in Rondonia, Western Amazon, Brazil. Environ. Pollut. 137, 179–186.

Almeida, M.D., Marins, R.V., Paraquetti, H.H.M., Bastos, W.R., Lacerda, L.D., 2009. Mercury degassing from forested and open field soils in Rondonia, Western Amazon, Brazil. Chemosphere 77, 60–66.

Bergquist, B.A., Blum, J.D., 2007. Mass-dependent and -independent fractionation of Hg isotopes by photoreduction in aquatic systems. Science 318, 417–420.

Blackwell, B.D., Driscoll, C.T., 2015. Deposition of Mercury in Forests along a Montane Elevation Gradient. Environ. Sci. Technol. 49, 5363–5370.

Blum, J.D., Sherman, L.S., Johnson, M.W., 2014. Mercury Isotopes in Earth and Environmental Sciences, in: Jeanloz, R. (Ed.), Annu Rev Earth Pl Sc, pp. 249–269.

Cao, M., Zou, X., Warren, M., Zhu, H., 2006. Tropical forests of Xishuangbanna, China. Biotropica 38, 306–309.

Carpi, A., Fostier, A.H., Orta, O.R., dos Santos, J.C., Gittings, M., 2014. Gaseous mercury emissions from soil following forest loss and land use changes: field experiments in the United States and Brazil. Atmos. Environ. 96, 423–429.

Cavanaugh, K.C., Gosnell, J.S., Davis, S.L., Ahumada, J., Boundja, P., Clark, D.B., Mugerwa, B., Jansen, P.A., O'Brien, T.G., Rovero, F., Sheil, D., Vasquez, R., Andelman, S., 2014. Carbon storage in tropical forests correlates with taxonomic diversity and functional dominance on a global scale. Glob. Ecol. Biogeogr. 23, 563–573.

Chen, J., Hintelmann, H., Feng, X., Dimock, B., 2012. Unusual fractionation of both odd and even mercury isotopes in precipitation from Peterborough, ON, Canada. Geochim. Cosmochim. Acta 90, 33–46.

Demers, J.D., Blum, J.D., Zak, D.R., 2013. Mercury isotopes in a forested ecosystem: Implications for air-surface exchange dynamics and the global mercury cycle. Glob. Biogeochem. Cycles 27, 222–238.

Demers, J.D., Driscoll, C.T., Fahey, T.J., Yavitt, J.B., 2007. Mercury cycling in litter and soil in different forest types in the Adirondack region, New York, USA. Ecol. Appl. 17, 1341–1351.

Driscoll, C.T., Mason, R.P., Chan, H.M., Jacob, D.J., Pirrone, N., 2013. Mercury as a global pollutant: sources, pathways, and effects. Environ. Sci. Technol. 47, 4967–4983.

Ericksen, J.A., Gustin, M.S., Schorran, D.E., Johnson, D.W., Lindberg, S.E., Coleman, J.S., 2003. Accumulation of atmospheric mercury in forest foliage. Atmos. Environ. 37, 1613–1622.

FAO, 2020. State World's For. 2021.

Fostier, A.H., Forti, M.C., Guimaraes, J.R.D., Melfi, A.J., Boulet, R., Santo, C.M.E., Krug, F.J., 2000. Mercury fluxes in a natural forested Amazonian catchment (Serra do Navio, Amapa State, Brazil). Sci. Total Environ. 260, 201–211.

Fostier, A.H., Melendez-Perez, J.J., Richter, L., 2015. Litter mercury deposition in the Amazonian rainforest. Environ. Pollut. 206, 605–610.

Frescholtz, T.F., Gustin, M.S., Schorran, D.E., Fernandez, G.C.J., 2003. Assessing the source of mercury in foliar tissue of quaking aspen. Environ. Toxicol. Chem. 22, 2114–2119.

Fu, X., Zhang, H., Liu, C., Zhang, H., Lin, C.-J., Feng, X., 2019. Significant seasonal variations in isotopic composition of atmospheric total gaseous mercury at forest sites in China caused by vegetation and mercury sources. Environ. Sci. Technol. 53, 13748–13756.

Gratz, L.E., Keeler, G.J., Blum, J.D., Sherman, L.S., 2010. Isotopic composition and fractionation of mercury in great lakes precipitation and ambient air. Environ. Sci. Technol. 44, 7764–7770.

Guedron, S., Arnouroux, D., Tessier, E., Grirnaldi, C., Barre, J., Berail, S., Perrot, V., Grimaldi, M., 2018. Mercury isotopic fractionation during pedogenesis in a tropical forest soil catena (French Guiana): deciphering the impact of historical gold mining. Environ. Sci. Technol. 52, 11573–11582.

Jiskra, M., Wiederhold, J.G., Skyllberg, U., Kronberg, R.-M., Hajdas, I., Kretzschmar, R., 2015. Mercury deposition and re-emission pathways in boreal forest soils investigated with Hg isotope signatures. Environ. Sci. Technol. 49, 7188–7196.

Kenzo, T., Inoue, Y., Yoshimura, M., Yamashita, M., Tanaka-Oda, A., Ichie, T., 2015. Height-related changes in leaf photosynthetic traits in diverse Bornean tropical rain forest trees. Oecologia 177, 191–202.

Kritee, K., Blum, J.D., Barkay, T., 2008. Mercury stable isotope fractionation during reduction of Hg(II) by different microbial pathways. Environ. Sci. Technol. 42, 9171–9177.

Kritee, K., Blum, J.D., Johnson, M.W., Bergquist, B.A., Barkay, T., 2007. Mercury stable isotope fractionation during reduction of Hg(II) to Hg(0) by mercury resistant microorganisms. Environ. Sci. Technol. 41, 1889–1895.

Li, K., Lin, C.-J., Yuan, W., Sun, G., Fu, X., Feng, X., 2019. An improved method for recovering and preconcentrating mercury in natural water samples for stable isotope analysis. J. Anal. At Spectrom. 34, 2303–2313.

Li, X., Wang, X., Yuan, W., Lu, Z., Wang, D., 2022. Increase of litterfall mercury input and sequestration during decomposition with a montane elevation in Southwest China. Environ. Pollut. 292, 292.

Lindberg, S., Bullock, R., Ebinghaus, R., Engstrom, D., Feng, X.B., Fitzgerald, W., Pirrone, N., Prestbo, E., Seigneur, C., 2007. A synthesis of progress and uncertainties in attributing the sources of mercury in deposition. Ambio 36, 19–32.

Lindberg, S.E., Stratton, W.J., 1998. Atmospheric mercury speciation: concentrations and behavior of reactive gaseous mercury in ambient air. Environ. Sci. Technol. 32, 49–57.

Lindqvist, O., Johansson, K., Aastrup, M., Andersson, A., Bringmark, L., Hovsenius, G., Hakanson, L., Iverfeldt, A., Meili, M., Timm, B., 1991. Mercury in the Swedish environment - recent research on causes, consequences and corrective methods. Water Air Soil Pollut. 55, R11–261.

Liu, W., Fox, J.E.D., Xu, Z., 2002. Biomass and nutrient accumulation in montane evergreen broad-leaved forest (Lithocarpus xylocarpus type) in Ailao Mountains, SW China. For. Ecol. Manag. 158, 223–235.

Lowry, B.E., Wittig, R.M., Pittermann, J., Oelze, V.M., 2021. Stratigraphy of stable isotope ratios and leaf structure within an African rainforest canopy with implications for primate isotope ecology. Sci. Rep. 11, 14222.

Lu, Z., Yuan, W., Luo, K., Wang, X., 2021. Litterfall mercury reduction on a subtropical evergreen broadleaf forest floor revealed by multi-element isotopes. Environ. Pollut. 268, 115867.

Lu, Z.Y., Wang, X., Zhang, Y.P., Zhang, Y.J., Luo, K., Sha, L.Q., 2016. High mercury accumulation in two subtropical evergreen forests in South China and potential determinants. J. Environ. Manag. 183, 488–496.

Lv, M., Luan, X., Liao, C., Wang, D., Liu, D., Zhang, G., Jiang, G., Chen, L., 2020. Human impacts on polycyclic aromatic hydrocarbon distribution in Chinese intertidal zones. Nat. Sustain. 3, 878–884.

Melendez-Perez, J.J., Fostier, A.H., Carvalho Jr., J.A., Windmoeller, C.C., Santos, J.C., Carpi, A., 2014. Soil and biomass mercury emissions during a prescribed fire in the Amazonian rain forest. Atmos. Environ. 96, 415–422.

Motta, L.C., Kritee, K., Blum, J.D., Tsz-Ki Tsui, M., Reinfelder, J.R., 2020. Mercury isotope fractionation during the photochemical reduction of Hg(II) coordinated with organic ligands. J. Phys. Chem. A 124, 2842–2853.

Obrist, D., Johnson, D.W., Edmonds, R.L., 2012. Effects of vegetation type on mercury concentrations and pools in two adjacent coniferous and deciduous forests. J. Plant Nutr. Soil Sci. 175, 68–77.

Obrist, D., Johnson, D.W., Lindberg, S.E., 2009. Mercury concentrations and pools in four Sierra Nevada forest sites, and relationships to organic carbon and nitrogen. Biogeosciences 6, 765–777.

Obrist, D., Kirk, J.L., Zhang, L., Sunderland, E.M., Jiskra, M., Selin, N.E., 2018. A review of global environmental mercury processes in response to human and natural perturbations: changes of emissions, climate, and land use. Ambio 47, 116–140.

Obrist, D., Roy, E.M., Harrison, J.L., Kwong, C.F., Munger, J.W., Moosmuller, H., Romero, C.D., Sun, S., Zhou, J., Commane, R., 2021. Previously unaccounted atmospheric mercury deposition in a midlatitude deciduous forest. Proc. Natl. Acad. Sci. U.S.A. 118, 118.

Pirrone, N., Cinnirella, S., Feng, X., Finkelman, R.B., Friedli, H.R., Leaner, J., Mason, R., Mukherjee, A.B., Stracher, G.B., Streets, D.G., Telmer, K., 2010. Global mercury emissions to the atmosphere from anthropogenic and natural sources. Atmos. Chem. Phys. 10, 5951–5964.

Rea, A.W., Lindberg, S.E., Scherbatskoy, T., Keeler, G.J., 2002. Mercury accumulation in foliage over time in two northern mixed-hardwood forests. Water Air Soil Pollut. 133, 49–67.

Richardson, J.B., Friedland, A.J., 2015. Mercury in coniferous and deciduous upland forests in northern New England, USA: implications of climate change. Biogeosciences 12, 6737–6749.

Rose, C.H., Ghosh, S., Blum, J.D., Bergquist, B.A., 2015. Effects of ultraviolet radiation on mercury isotope fractionation during photo-reduction for inorganic and organic mercury species. Chem. Geol. 405, 102–111.

Roulet, M., Lucotte, M., Farella, N., Serique, G., Coelho, H., Passos, C.J.S., Silva, E.D.J.D., Andrade, P.S.D., Mergler, D., Guimarães, J.R.D., 1999. Effects of recent human colonization on the presence of mercury in Amazonian ecosystems. Water Air Soil Pollut. 112, 297–313.

Roulet, M., Lucotte, M., Saint-Aubin, A., Tran, S., Rheault, I., Farella, N., Da Silva, E.D., Dezencourt, J., Passos, C.J.S., Soares, G.S., Guimaraes, J.R.D., Mergler, D., Amorim, M., 1998. The geochemistry of mercury in central Amazonian soils developed on the Alter-do-Chao formation of the lower Tapajos River Valley, Para state, Brazil. Sci. Total Environ. 223, 1–24.

Sherman, L.S., Blum, J.D., Johnson, K.P., Keeler, G.J., Barres, J.A., Douglas, T.A., 2010. Mass-independent fractionation of mercury isotopes in Arctic snow driven by sunlight. Nat. Geosci. 3, 173–177.

Silva, E.V., Machado, W., Oliveira, R.R., Sella, S.M., Lacerda, L.D., 2006. Mercury deposition through litterfall in an Atlantic Forest at Ilha Grande, southeast Brazil. Chemosphere 65, 2477–2484.

Skyllberg, U., Bloom, P.R., Qian, J., Lin, C.M., Bleam, W.F., 2006. Complexation of mercury(II) in soil organic matter: EXAFS evidence for linear two-coordination with reduced sulfur groups. Environ. Sci. Technol. 40, 4174–4180.
Strassburg, B.B.N., Kelly, A., Balmford, A., Davies, R.G., Gibbs, H.K., Lovett, A., Miles, L., Orme, C.D.L., Price, J., Turner, R.K., Rodrigues, A.S.L., 2010. Global congruence of carbon storage and biodiversity in terrestrial ecosystems. Conserv. Lett. 3, 98–105.
Sun, G.Y., Sommar, J., Feng, X.B., Lin, C.J., Ge, M.F., Wang, W.G., Yin, R.S., Fu, X.W., Shang, L.H., 2016. Mass-Dependent and -Independent Fractionation of Mercury Isotope during Gas-Phase Oxidation of Elemental Mercury Vapor by Atomic Cl and Br. Environ. Sci. Technol. 50, 9232–9241.
Teixeira, D.C., Lacerda, L.D., Silva-Filho, E.V., 2017. Mercury sequestration by rainforests: The influence of microclimate and different successional stages. Chemosphere 168, 1186–1193.
Teixeira, D.C., Lacerda, L.D., Silva-Filho, E.V., 2018. Foliar mercury content from tropical trees and its correlation with physiological parameters in situ. Environ. Pollut. 242, 1050–1057.
Teixeira, D.C., Montezuma, R.C., Oliveira, R.R., Silva, E.V., 2012. Litterfall mercury deposition in Atlantic forest ecosystem from SE - Brazil. Environ. Pollut. 164, 11–15.
Tuomi, M., Thum, T., Järvinen, H., Fronzek, S., Berg, B., Harmon, M., Trofymow, J.A., Sevanto, S., Liski, J., 2009. Leaf litter decomposition—Estimates of global variability based on Yasso07 model. Ecol. Model. 220, 3362–3371.
Walkley, A., 1947. A Critical examination of a rapid method for determining organic carbon in soils—Effect of variations in digestion conditions and of inorganic soil constituents. Soil Sci. 63, 63–264.
Wang, X., Bao, Z., Lin, C.-J., Yuan, W., Feng, X., 2016a. Assessment of global mercury deposition through litterfall. Environ. Sci. Technol. 50, 8548–8557.
Wang, X., Lin, C.J., Lu, Z.Y., Zhang, H., Zhang, Y.P., Feng, X.B., 2016b. Enhanced accumulation and storage of mercury on subtropical evergreen forest floor: Implications on mercury budget in global forest ecosystems. J. Geophys. Res. -Biogeosci. 121, 2096–2109.
Wang, X., Lin, C.J., Yin, R., Yuan, W., Lin, C.-J., Sommar, J., Feng, X., Wang, H., Lin, C., 2017. Using mercury isotopes to understand mercury accumulation in the montane forest floor of the Eastern Tibetan Plateau. Environ. Sci. Technol. 51, 801–809.
Wang, X., Luo, J., Yuan, W., Lin, C.J., Wang, F., Liu, C., Wang, G., Feng, X., 2020a. Global warming accelerates uptake of atmospheric mercury in regions experiencing glacier retreat. Proc. Natl. Acad. Sci. U.S.A. 117, 2049–2055.
Wang, X., Yuan, W., Lin, C.-J., Feng, X., 2021. Mercury cycling and isotopic fractionation in global forests. Crit. Rev. Environ. Sci. Technol. 11, 1–24.
Wang, X., Yuan, W., Lin, C.J., Luo, J., Wang, F., Feng, X., Fu, X., Liu, C., 2020b. Underestimated sink of atmospheric mercury in a deglaciated forest chronosequence. Environ. Sci. Technol. 54, 8083–8093.
Wang, X., Yuan, W., Lin, C.J., Zhang, L.M., Zhang, H., Feng, X.B., 2019a. Climate and vegetation as primary drivers for global mercury storage in surface soil. Environ. Sci. Technol. 53, 10665–10675.
Wang, X., Yuan, W., Lu, Z., Lin, C.-J., Yin, R., Li, F., Feng, X., 2019b. Effects of precipitation on mercury accumulation on subtropical montane forest floor: implications on climate forcing. J. Geophys. Res.: Biogeosci. 124, 959–972.
Xia, S.-W., Chen, J., Schaefer, D., Detto, M., 2015. Scale-dependent soil macronutrient heterogeneity reveals effects of litterfall in a tropical rainforest. Plant Soil 391, 51–61.
Yin, K., Wang, Q., Lv, M., Chen, L., 2019. Microorganism remediation strategies towards heavy metals. Chem. Eng. J. 360, 1553–1563.
Yuan, W., Sommar, J., Lin, C.-J., Wang, X., Li, K., Liu, Y., Zhang, H., Lu, Z., Wu, C., Feng, X., 2019. Stable isotope evidence shows re-emission of elemental mercury vapor occurring after reductive loss from foliage. Environ. Sci. Technol. 53, 651–660.
Yuan, W., Wang, X., Lin, C.J., Sommar, J.O., Wang, B., Lu, Z., Feng, X., 2021. Quantification of atmospheric mercury deposition to and legacy re-emission from a subtropical forest floor by mercury isotopes. Environ. Sci. Technol. 55, 12352–12361.
Yuan, W., Wang, X., Lin, C.J., Wu, C., Zhang, L., Wang, B., Sommar, J., Lu, Z., Feng, X., 2020. Stable mercury isotope transition during postdepositional decomposition of biomass in a forest ecosystem over five centuries. Environ. Sci. Technol. 54, 8739–8749.
Zheng, W., Demers, J.D., Lu, X., Bergquist, B.A., Anbar, A.D., Blum, J.D., Gu, B., 2019. Mercury stable isotope fractionation during abiotic dark oxidation in the presence of thiols and natural organic matter. Environ. Sci. Technol. 53, 1853–1862.
Zheng, W., Hintelmann, H., 2009. Mercury isotope fractionation during photoreduction in natural water is controlled by its Hg/DOC ratio. Geochim. Et Cosmochim. Acta 73, 6704–6715.
Zheng, W., Hintelmann, H., 2010a. Isotope fractionation of mercury during its photochemical reduction by low-molecular-weight organic compounds. J. Phys. Chem. A 114, 4246–4253.
Zheng, W., Hintelmann, H., 2010b. Nuclear field shift effect in isotope fractionation of mercury during abiotic reduction in the absence of light. J. Phys. Chem. A 114, 4238–4245.
Zheng, W., Obrist, D., Weis, D., Bergquist, B.A., 2016. Mercury isotope compositions across North American forests. Glob. Biogeochem. Cycles 30, 1475–1492.
Zhou, J., Obrist, D., 2021. Global mercury assimilation by vegetation. Environ. Sci. Technol. 55, 14245–14257.